Science Arts & Métiers (SAM)
is an open access repository that collects the work of Arts et Métiers Institute of Technology researchers and makes it freely available over the web where possible.

This is an author-deposited version published in: https://sam.ensam.eu
Handle ID: .http://hdl.handle.net/10985/17377

To cite this version :

David BUSSON, Richard BEAREE, Adel OLABI - Task-oriented rigidity optimization for 7 DOF redundant manipulators - In: 20th IFAC World Congress, France, 2017-07 - IFAC WORLD CONGRESS SPECIAL ISSUE - 2017

Any correspondence concerning this service should be sent to the repository Administrator : archiveouverte@ensam.eu

Task-oriented rigidity optimization for 7 DOF redundant manipulators

D. Busson, R. Bearee, A. Olabi

Arts et Metiers, LSIS CNRS 7296, 8 *Bd Louis XIV*, 59046 *Lille,*
FRANCE (e-mail: david.busson@ensam.eu, richard.bearee@ensam.eu,
adel.olabi@ensam.eu).

Abstract: In this work, redundancy resolution has been employed to increase the Cartesian mechanical rigidity of 7 DOF robot manipulators during tasks requiring stiff interactions with the environment (e.g. milling or drilling). The Cartesian static stiffness of the end-effector for a given joint configuration is deduced from an identified joints stiffness model. The Cartesian reflected rigidity evolution over an analytically computed self-motion of the manipulator shows significant variations that clearly highlight the need to select the right set of joint angles among the possible ones. A global optimization scheme of the redundant DOF is proposed to determine the stiffest robot configurations for a given pose of the end-effector. An experimental study on 7 DOF KUKA LBR iiwa then shows the relevance of the proposed approach in finding the redundant robot joint angles that optimize this rigidity criteria.

Keywords: Kinematic redundancy; Joint stiffness; Cartesian rigidity; 7 DOF anthropomorphic robot arm.

1. INTRODUCTION

Up until recently, industrial robots were mainly used for repetitive, heavy or dangerous works. The new generation of industrial collaborative robots opens the door to numerous operating scenarios [Cherubini et al. (2016)]. Even if current examples of effective human-robot collaboration are restricted, the safe shared workspace between human and robot is a key factor of flexibility for this new kind of industrial robotics. A second advantage for some robots, beyond the safety certification, is their embedded compliant behavior, which significantly simplifies the implementation of tasks involving soft interactions with the environment, such as assembly tasks. Now, to accomplish specific tasks such as milling, drilling (see Fig. 1) or lifting loads, the limited payload of the current industrial collaborative robots can be very restrictive. In this case, it would be interesting to use the mechanically stiffest robot configuration regarding the force or torque imposed by the task-space interactions.

Considering the case of 7 DOF anthropomorphic robotic arms, the self-motion capacity induced by the redundant DOF offers the opportunity of optimizing the Cartesian rigidity for a given end-effector pose. A lot of work has already been done concerning the Cartesian impedance control techniques for robots, using for instance the Cartesian stiffness ellipsoid or the manipulability ellipsoid [Yoshikawa. (1985); Albu-Schaffer et al. (2003); Kurazume and T. Hasegawa. (2006); Ficuciello et al. (2015)] to define the control parameters in an arbitrary non-singular configuration to match with a desired end-effector behavior. In [Ajoudani et al. (2015)], the authors show that using the previous approaches the suitable selection of a configuration within the self-motion could be underestimated. Then, they explore the influence of different robot configurations and propose a configuration-dependant stiffness control method exploiting redundancy resolution to achieve a desired task-space interaction behavior.

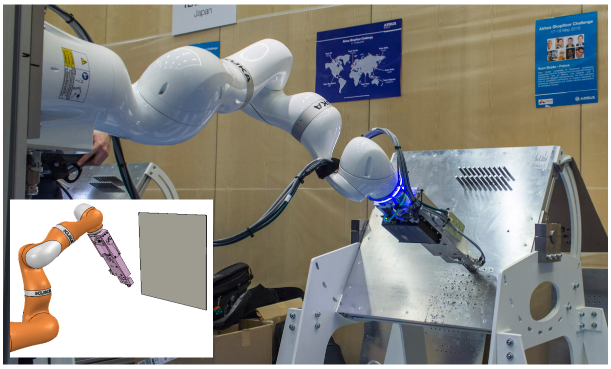

Fig. 1. Kuka LBR iiwa used for aerospace drilling operations. View of our robotic system (team SIRADO) during the Airbus Shopfloor Challenge [Airbus/ICRA. (2016)].

This paper aims at contributing to this field by presenting a practical use of the self-motion of a redundant manipulator for the global maximization of the Cartesian static rigidity. This is particularly interesting when dealing with positioning tasks such as drilling operations. The main assumption is that the robot joints are locked or at rest in position control mode at a certain posture, i.e. that the tool feed is carried out by the end-effector. The optimization of elastostatic performances are based on an analytical inverse model of a 7 DOF robotic arm and a configuration-based Cartesian stiffness model. After highlighting the redundant DOF strong influence on the Cartesian rigidity components, an experimental study on the KUKA LBR iiwa is presented.

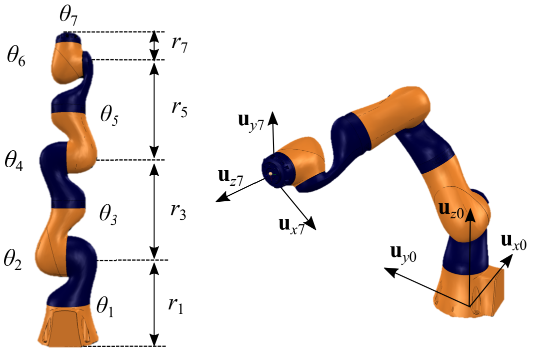

Fig. 2. Parameters of the Kuka LBR iiwa in initial configuration and end-effector frame.

2. CLOSED-FORM INVERSE KINEMATIC MODEL FOR THE KUKA LBR IIWA ROBOT

2.1 Robot kinematic model

Table 1. LBR iiwa DH parameters

i	α_i (rad)	θ_i (rad)	d_i (mm)	r_i (mm)
1	0	θ_1	0	360
2	$-\pi/2$	θ_2	0	0
3	$\pi/2$	θ_3	0	420
4	$\pi/2$	θ_4	0	0
5	$-\pi/2$	θ_5	0	400
6	$-\pi/2$	θ_6	0	0
7	$\pi/2$	θ_7	0	126

The Kuka LBR iiwa is a seven degrees-of-freedom (DOF) manipulator. Hence, the robot manipulator is kinematically redundant, with a least one redundant DOF, with respect to the task dimension. Table 1 gives the modified D-H parameters [Khalil and Dombre. (1990)] provided by the robot manufacturer. Noting $\mathbf{q} = [\theta_1, \cdots, \theta_7]^\top$ the (7×1) joint position vector, the forward kinematic of the robot, i.e. the position vector $\mathbf{p}$ and the unit vectors $\mathbf{n}$, $\mathbf{m}$ and $\mathbf{w}$ of the end-effector frame with respect to the base frame (see Fig. 2), can be expressed as

$$\mathbf{T}(\mathbf{q}) = \prod_{i=1}^{7} \mathbf{H}_i(\theta_i) = \begin{pmatrix} \mathbf{n} & \mathbf{m} & \mathbf{w} & \mathbf{p} \\ 0 & 0 & 0 & 1 \end{pmatrix}, \tag{1}$$

with $\mathbf{H}_i$ the homogeneous transformation matrix

$$\mathbf{H}_i(\theta_i) = \begin{pmatrix} c_{\theta_i} & -c_{\alpha_i} s_{\theta_i} & s_{\alpha i} s_{\theta_i} & a_i c_{\theta_i} \\ s_{\theta_i} & c_{\alpha_i} s_{\theta_i} & -s_{\alpha i} s_{\theta_i} & a_i s_{\theta_i} \\ 0 & s_{\alpha i} & c_{\alpha_i} & d_i \\ 0 & 0 & 0 & 1 \end{pmatrix}, \tag{2}$$

where c_ϕ and s_ϕ respectively stand for $\cos(\phi)$ and $\sin(\phi)$.

Noting $\mathbf{x} = [\mathbf{p}\ \varphi]$ the (6×1) end-effector position vector, with φ the orientation of the end-effector calculated from the vectors $\mathbf{n}$, $\mathbf{m}$ and $\mathbf{w}$ (e.g. using the Euler angles parametrization), we can also defined the classical mapping

$$\dot{\mathbf{x}} = \mathbf{J}(\mathbf{q}) \cdot \dot{\mathbf{q}}, \tag{3}$$

which relates the joint velocity vector $\dot{\mathbf{q}}$ to the end-effector Cartesian velocity vector $\dot{\mathbf{x}}$ through the (6×7) Jacobian matrix $\mathbf{J}(\mathbf{q})$.

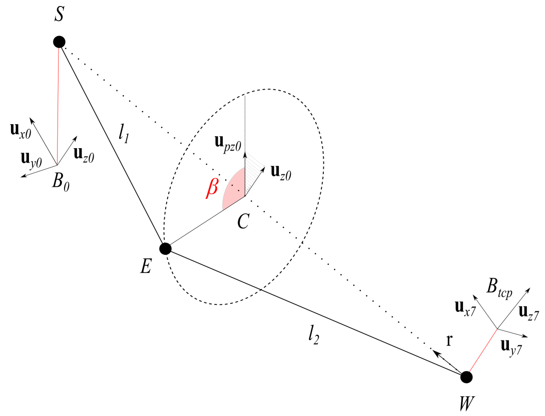

Fig. 3. Self-motion of 7 DOF S-R-S anthropomorphic arms: elbow constrained to a circle.

2.2 Closed-form Inverse Kinematic model

Dahm and Joublin [Dahm and Joublin. (1997)] were among the firsts to introduce an analytical solution to the inverse geometric problem of 7 DOF anthropomorphic arms. Their method was based on the fact that this type of redundant arm may be divided into a succession of 2 DOF spherical articulations, built from the fusion of two successive roll and pitch revolute joints, and one revolute joint for the ultimate axis. For a given pose of the tip of this anthropomorphic arm, the 2 DOF elbow articulation is shown to be constrained to a circle. The method we use for this work is based on the formulation given by Tolani in [Tolani et al. (2000)], which provides another decomposition of the iiwa-type robot arm. In this method, the fusion of the first three and the last three joints make respectively a 3 DOF shoulder spherical joint (positioned in S in Fig. 3) and a 3 DOF wrist spherical joint (in W). The forth revolute axis of the kinematic chain is then taken as it is, and is called the elbow (in E).

Variations of these methods were further studied in [Moradi and Lee. (2008)] and [Shimizu et al. (2006)], where the admissible positions of the elbow within the circle were determined taking into account the joint limits. A use of this method is performed in [Wang and Artemiadis. (2014)] to mimic the natural motions of a human arm with an anthropomorphic robotic arm by applying a measured equivalent redundancy angle. In [Zhou et al. (2015)], the same analytical method is used for anthropomorphic robots sent in space. A redundancy resolution is performed to minimize the disturbances induced by the kinematic structure on the manipulator base.

In a given configuration, the elbow is located at a constant distances l_1 from the shoulder and l_2 from the wrist. Hence, the elbow lies onto two spheres, of respective radii l_1 and l_2, centered at the shoulder and at the wrist. The intersection of these two spheres is a circle centered at the shoulder-wrist axis, and that lies in a plane whose normal is parallel to this same axis. The tangent of this circle gives the direction of the elbow rotation axis. The Cartesian position of the elbow on this circle allows for a parametrization of the one dimensional self-motion of this type of redundant manipulator. Dahm and Joublin [Dahm and Joublin. (1997)] use the term of “redundancy angle” while Tolani [Tolani et al. (2000)] uses “swivel angle” to parametrize the position of the elbow. This redundancy parameter, here called β, is the angular measure between the vector going from the center of the self-motion circle to the elbow to the projection ($\mathbf{u}_{pz0}$) of an arbitrary vector (here, $\mathbf{u}_{z0}$) on the plane of the self-motion. Noting $\mathbf{r} = \frac{\mathbf{SW}}{\|\mathbf{SW}\|}$ the unit vector directing the shoulder-wrist axis, $l_1' = \|\mathbf{SC}\| = \frac{\|\mathbf{SW}\|^2 - {l_2}^2 + {l_1}^2}{2\|\mathbf{SW}\|}$ the distance from the shoulder to the center of the circle and $R = \sqrt{{l_1}^2 - {l_1'}^2}$ the radius of the circle, we can write the influence of the redundancy angle β over the position of the elbow E as :

$$E = S - l_1'\mathbf{r} + R(\cos\beta\mathbf{u}_{pz0} + \sin\beta(\mathbf{u}_{pz0} \wedge \mathbf{r})) \qquad (4)$$

Picking a redundancy angle for the elbow provides an additional constraint to the task, then the iiwa-type robot is not anymore redundant and a closed form solution exists. After computing the Cartesian positions of the shoulder, wrist and elbow thanks to the value of the robot base frame, the destination frame, and β, the analytical method used for the inverse geometry of the LBR iiwa is divided into three steps: 1) Determination of the forth axis angle from a cosine rule in the Shoulder-Elbow-Wrist triangle. 2) Computation of the robot-base-to-elbow-base relative rotation and of the elbow-base-to-wrist-base relative rotation, respectively corresponding to the rotations achieved by the 3 DOF spherical shoulder and the 3 DOF spherical wrist. 3) Determination of the articular angles composing each 3 DOF spherical articulations of the robot to achieve the rotations computed at the former step.

The analytical computation of articular configurations fc a given pose of the ultimate link over a $[0, 2\pi]$ range (uniform sampling of β provides a representative overvie of the self-motion of the robot. It is then possible t assess configuration-based performance criterion over representation of the self-motion of the robot.

3. REDUNDANCY RESOLUTION WITH RIGIDITY OPTIMIZATION

3.1 Cartesian compliance model

For most industrial robots, joints compliance and more specifically gears compliance is recognized as the main mechanical source of deformation during robot motion and during robot-environment interaction [Wu et al. (2012); Lee. (2013)]. In this study, the joints radial deformation is neglected and, as described in Fig. 4, the joint compliance is modeled as a torsion spring with stiffness value noted $k_{q,i}$ for each joint i. Hence, the joint rigidity matrix $\mathbf{K}_q$ is a square (7×7) diagonal matrix with the elements $k_{q,i}$ on the main diagonal. The static joints stiffness values of a robot can be experimentally determined by comparing each joint angular variation to a set of imposed external forces or torques. In the case of the Kuka LBR iiwa, the embedded joint torque sensors can be advantageously exploited to simplify the joint stiffness identification procedure as detailed in [Besset et al. (2016)]. One notes that the reflected stiffness values for one joint is the result of the serial combination of the gears stiffness value and the equivalent control stiffness value. Therefore, the joint stiffness values are dependent on the robot control mode. For instance, the impedance control mode[1] will induced lower joint stiffness values than the position control mode. The focus of this study being the maximization of the reflected stiffness, the position control mode is considered. Fig. 5 describes the experimental measurement of the joint 2 stiffness in position control mode (position hold) and in locked joint-brake mode for the Kuka LBR iiwa 14R820. It should be noted that the identified stiffness value in position control mode is very close to the static gear stiffness value. The measured values of the 7 joint stiffness in position control mode are given in Table 2.

Table 2. Identified joint stiffness values of the Kuka LBR iiwa 14R820 (Nm/rad)

$k_{q,1}$	$k_{q,2}$	$k_{q,3}$	$k_{q,4}$	$k_{q,5}$	$k_{q,6}$	$k_{q,7}$
4.2e4	3.96e4	1.22e4	2.02e4	0.8e4	0.38e4	0.48e4

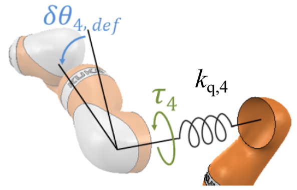

Fig. 4. Example of joint model (joint 4). The i^{th} joint compliance is modeled as a torsion spring with stiffness $k_{q,i}$.

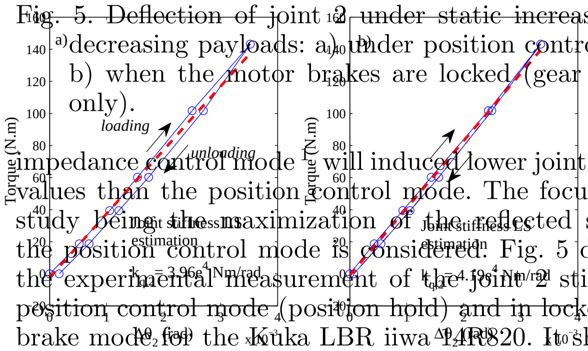

Fig. 5. Deflection of joint 2 under static increasing and decreasing payloads: a) under position control mode, b) when the motor brakes are locked (gear stiffness only).

Defining the joint compliance matrix $\mathbf{C}_q = \mathbf{K}_q^{-1}$, the relation between the (7×1) joint displacement vector $\delta\mathbf{q}$ and the (7×1) vector of the joint static torques $\boldsymbol{\tau}$ may be expressed as

$$\delta\mathbf{q} = \mathbf{C}_q \cdot \boldsymbol{\tau}. \qquad (5)$$

Clearly, the resulting end-effector compliance will be induced by the joint stiffness values and will depend on the robot configuration. Noting $\mathbf{C}_x(\mathbf{q})$ the Cartesian compliance matrix at the end-effector, the relation between the (6×1) static Cartesian force-torque vector F acting at the end-effector and the (6×1) end-effector displacement vector $\delta\mathbf{x}$ (translation and rotation) can be written

$$\delta\mathbf{x} = \mathbf{C}_x(\mathbf{q}) \cdot \mathbf{F}. \qquad (6)$$

---

[1] The user-selected joint or Cartesian stiffness are less or almost equal to the position controlled mode equivalent stiffness.

Now, considering that the joint compliance matrix $\mathbf{C}_q$ is known, i.e. that the 7 robot joints compliance $1/k_{q,i}$ are identified, the Cartesian compliance $\mathbf{C}_x$ can be analytically deduced. Applying the principle of energy conservation to the robot [Khatib. (1990)], associated to the principle of virtual work, and neglecting the works of gravitational and frictional forces leads to the relation

$$\delta W_\tau = \boldsymbol{\tau}^\top \cdot \delta\mathbf{q} = \delta W_F = \mathbf{F}^\top \cdot \delta\mathbf{x}, \tag{7}$$

with δW_τ and δW_F respectively the virtual work of the joint torques and the virtual work associated to the external force. Substituting the Cartesian and joint displacement into the kinematic relation deduced from equation (3) for small displacement

$$\delta\mathbf{x} = \mathbf{J}(\mathbf{q}) \cdot \delta\mathbf{q}, \tag{8}$$

with equation (5) and equation (6) leads to the relation

$$\mathbf{C}_x(\mathbf{q}) \cdot \mathbf{F} = \mathbf{J}(\mathbf{q}) \cdot \mathbf{C}_q \cdot \boldsymbol{\tau}. \tag{9}$$

Finally, substituting the joint torque $\boldsymbol{\tau}$ with equation (7) into equation (9) allows to calculate the robot Cartesian compliance matrix according to the identified joint compliance matrix

$$\mathbf{C}_x(\mathbf{q}) = \mathbf{J}(\mathbf{q}) \cdot \mathbf{C}_q \cdot \mathbf{J}^\top(\mathbf{q}). \tag{10}$$

One can note that the previous relation represents a mapping of the compliance in the redundant joint space into the robot operational space without the need for the calculus of a generalized Jacobian inverse matrix. The Cartesian compliance matrix given by equation (10) can be used to evaluate the mechanical compliant behavior of the robot submitted to an external force at the end-effector according to the robot configuration. This mechanical compliance metrics can be advantageously used to find the stiffest configuration of the redundant robot for a given force or torque direction imposed by the operational task.

3.2 *Redundancy and rigidity*

The problem of finding the stiffest configuration for a redundant robot can be locally addressed using a redundancy resolution based on a generalized jacobian inverse (classically the Moore-Penrose inverse) for the end-effector configuration and by projecting the gradient of the rigidity cost function onto the null space of the manipulator Jacobian. In this work, we take advantage of the existence of the analytical inverse model of the 7DOF anthropomorphic arm, described in section 2.2, to easily find the global solution of the rigidity optimization problem.

The Cartesian compliance matrix $\mathbf{C}_x$ given by equation (10) is a (6×6) matrix with positive diagonal terms. We define the (3×1) Cartesian translation stiffness vector $\mathbf{k}_{trans}$ and the (3×1) Cartesian rotation stiffness vector $\mathbf{k}_{rot}$ as being composed of the first three and the last three inverse of the diagonal terms of the compliance matrix. Writing $\mathbf{C}_x = (c_{x_{ij}})_{i,j \in [\![1,6]\!]^2}$, we have :

$$\mathbf{k}_{trans} \triangleq \begin{bmatrix} 1/c_{x_{11}} \\ 1/c_{x_{22}} \\ 1/c_{x_{33}} \end{bmatrix} ; \ \mathbf{k}_{rot} \triangleq \begin{bmatrix} 1/c_{x_{44}} \\ 1/c_{x_{55}} \\ 1/c_{x_{66}} \end{bmatrix}. \tag{11}$$

We define two (3×1) unit vectors $\boldsymbol{\eta}_{trans}$ and $\boldsymbol{\eta}_{trans}$ whose components respectively correspond to the translational or rotational directions in which single-objective rigidity optimization is desired. Therefore, the translational (respectively rotational) rigidity optimization for a given end-effector pose, consists in finding the redundancy parameter β_{trans} (resp. β_{rot}), which maximizes the Cartesian translation (resp. rotation) stiffness $\mathbf{k}_{trans}$ (resp. $\mathbf{k}_{rot}$) along the direction given by $\boldsymbol{\eta}_{trans}$ (resp. $\boldsymbol{\eta}_{trans}$). The optimized redundancy angle for a desired translational or rotational stiffness can be expressed as:

$$\beta_{trans} = \underset{\beta \in [0\ \ 2\pi]}{\arg\max} \left(\mathbf{k}_{trans}^\top(\mathbf{q}) \cdot \boldsymbol{\eta}_{trans}\right), \tag{12}$$

and

$$\beta_{rot} = \underset{\beta \in [0\ \ 2\pi]}{\arg\max} \left(\mathbf{k}_{rot}^\top(\mathbf{q}) \cdot \boldsymbol{\eta}_{rot}\right). \tag{13}$$

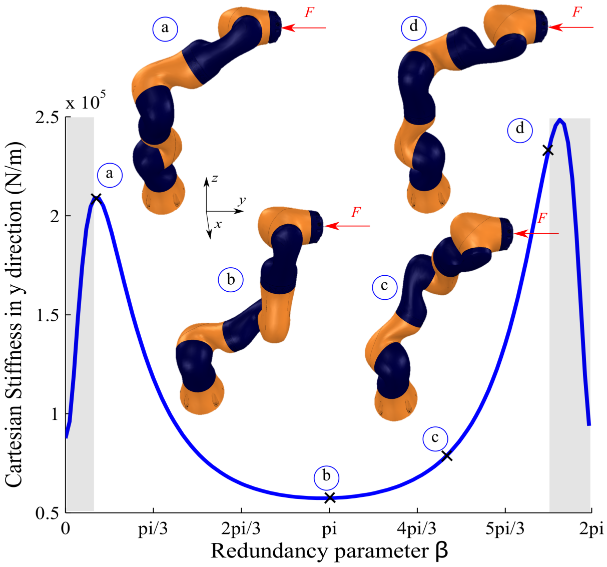

Fig. 6. Theoretical Cartesian stiffness along pure y translational direction over a $[0, 2\pi]$ range of β. Example for the end-effector pose $\mathbf{x} = [0,\ .5,\ .975,\ 0,\ \pi/2,\ -\pi/2]^\top$.

3.3 *Case studies*

For all presented cases, the shaded areas on the figures indicate the inaccessible self-motion parameter β, which are calculated according to the joint-limits of the studied robot.

Fig. 6 shows the evolution of the Cartesian stiffness along translational y-direction (in robot base reference frame) over a $[0, 2\pi]$ range of β for a given end-effector position and orientation $\mathbf{x}$. Among the four robot configurations shown in the figure, the stiffest configurations ⓐ and ⓓ and the most flexible ones ⓑ and ⓒ, may be intuitively determined. One can note that the rigidity gain between the stiffest configuration and the softest configuration is almost 400%. This result illustrates the significant influence of the robot self-motion on the mechanical rigidity of the end-effector. Regarding the two stiffest configurations ⓐ and ⓓ, the difference between both configurations is less intuitive, but the rigidity gain of choosing ⓐ over ⓓ is still of 20%.

Fig. 7 shows the evolution of the linear components of the Cartesian stiffness for a different end-effector pose. For this pose, the Cartesian stiffness along y-direction is mainly influenced by joint 4 position, while the stiffness in x-direction and z-direction are dominated by the imposed constraints on joint 3. Succession of single local

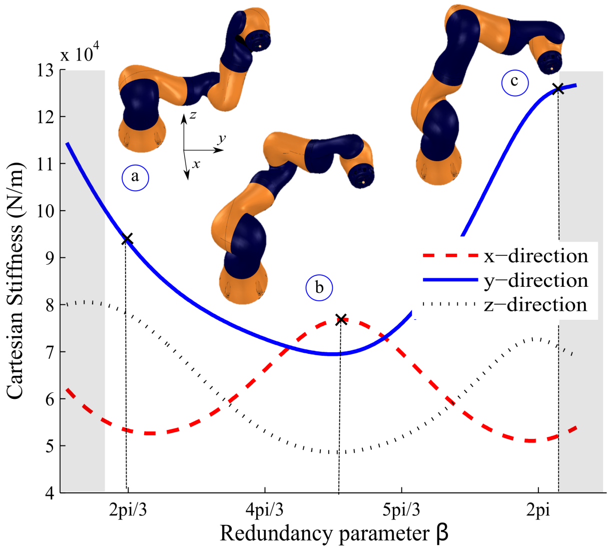

Fig. 7. Theoretical linear Cartesian stiffness evolution according to the redundancy parameter β for the static end-effector pose $\mathbf{x} = [-.2,\ .5,\ .6,\ 0,\ -\pi/2,\ \pi]^\top$.

operations along one Cartesian axis are in widespread use in the aerospace or automotive manufacturing industries. Fig. 8 and Fig. 9 presents the evolution of the Cartesian stiffness value in y-direction according to the redundancy parameter and the position of the end-effector along the x-axis. Fig. 8 shows that the redundancy parameter could be sequentially modified during the motion to maximize the rigidity along y-direction on every operation poses corresponding to changing x values. For practical efficiency of the successive operations, e.g. for repeatability reason, it would be more convenient to keep the optimized rigidity value as constant as possible for each operation. Fig. 9 shows the resulting maximum iso-rigidity curve in the $x\beta$-plane for the considered example.

4. EXPERIMENTAL RESULTS

Fig. 10 describes the experimental Setup. For a set of imposed end-effector pose of the KUKA LBR iiwa 14 R820 manipulator, a known external load (0, 4 and 10 kg) was applied to the robot end-effector in the studied direction. The self-motion of the robot was obtained by imposing a stepwise variation (steps of 5 degrees) of the external redundant joint 3 for the imposed end-effector pose. Then, the deviation of the end-effector was measured by a laser tracker from API Inc. with absolute accuracy of $\pm 15\ \mu$m/m. The Cartesian rigidity values were first measured over a range of joint 3 angle values. They were then re-parametrized with regards to the redundancy parameter β (for better comparison with previously described analytical model).

Fig. 11 presents samples of experimental results for two different end-effector poses. It can be observed that the general behavior (general trend, minima and maxima) predicted by the analytical Cartesian stiffness model was corroborated by the experiments. Hence, the validity of the identified joint stiffness model for this robot is confirmed and the proposed Cartesian static stiffness optimization can be efficiently used for practical applications.

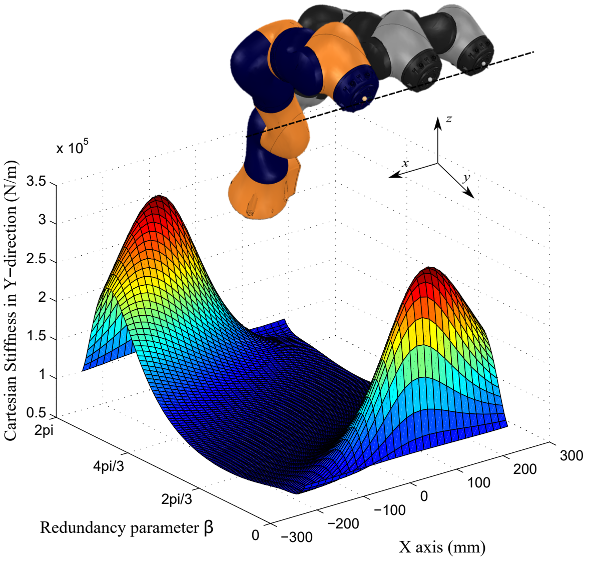

Fig. 8. Theoretical Cartesian stiffness along pure y translational direction over a $[0, 2\pi]$ range of β and a $[-.25, .25]$ range of x. $\mathbf{x} = [x,\ .5,\ .975,\ 0,\ \pi/2,\ -\pi/2]^\top$.

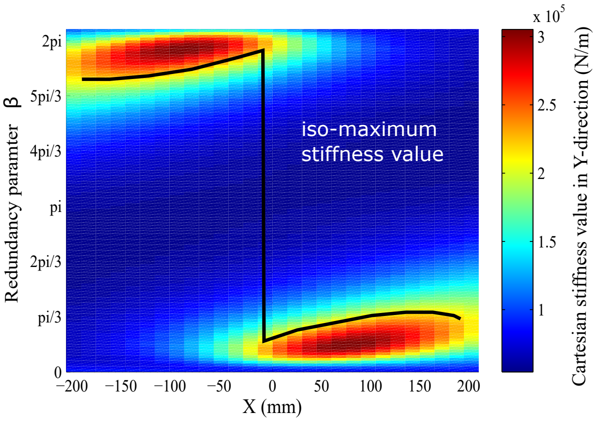

Fig. 9. Maximum iso-rigidity curve for the motion of Fig. 8.

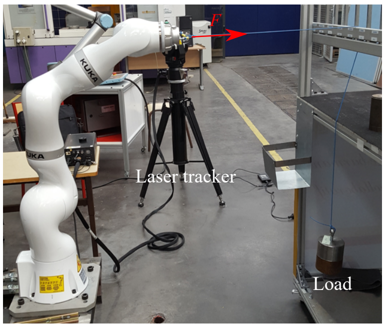

Fig. 10. Experimental setup. KUKA LBR iiwa 14 R820 arm, API laser tracker and example of payload acting in y-direction.

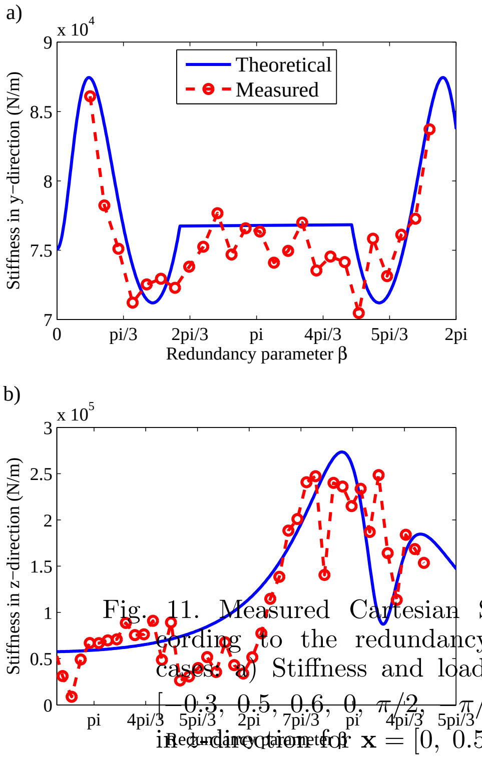

Fig. 11. Measured Cartesian Stiffness component according to the redundancy angle β for two test cases: a) Stiffness and load in y-direction for $\mathbf{x} = [-0.3,\ 0.5,\ 0.6,\ 0,\ \pi/2,\ -\pi/2]^\top$; b) Stiffness and load in z-direction for $\mathbf{x} = [0,\ 0.5,\ 0.5,\ -\pi,\ 0,\ \pi]^\top$.

5. CONCLUSION

In this paper, redundancy resolution of 7 DOF anthropomorphic arms for determining the stiffest static configuration regarding the task-space interactions has been treated. The optimization is based on an analytically computed self-motion that take account of an identified joint stiffness model. Analytical and experimental results obtained on a KUKA LBR iiwa for a given pose demonstrated the strong influence of the redundant DOF on the Cartesian stiffness. Finally, the proposed approach gives an efficient and convenient way to select the joint configuration of 7 DOF manipulator for tasks requiring stiff interactions.

ACKNOWLEDGEMENTS

This work is supported by the European Community, under Horizon 2020 grants 6888807 “COLROBOT” (Collaborative Robotics for Assembly and Kitting in Smart Manufacturing).

REFERENCES

Airbus Shopfloor Challenge, 2016. *www.airbusgroup.com/airbusshopfloorchallenge*

A. Ajoudani, N. G. Tsagarakis and A. Bicchi. On the role of robot configuration in Cartesian stiffness control. *In Proc. of IEEE International Conference on Robotics and Automation (ICRA)*, Seattle, WA, 1010–1016, 2015.

A. Albu-Schaffer, C. Ott, U. Frese and G. Hirzinger. Cartesian impedance control of redundant robots: recent results with the DLR-light-weight-arms. *In Proc. of IEEE International Conference on Robotics and Automation (ICRA)*, Taipei, Taiwan, 3704–3709, 2003.

P. Besset, A. Olabi and O. Gibaru. Advanced calibration applied to a collaborative robot. *In Proc. of IEEE International Power Electronics and Motion Control Conference*, Varna, Bulgaria, 2016.

A. Cherubini, R. Passama, A. Crosnier, A. Lasnier and Ph. Fraisse. Collaborative manufacturing with physical humanrobot interaction *Robotics and Computer-Integrated Manufacturing*, Vol. 40, 1–13, 2016.

P. Dahm and F. Joublin. Closed form solution for the inverse kinematics of a redundant robot arm. *Inst. Neuroinf*, Ruhr Univ. Bochum, 1997.

F. Ficuciello, L. Villani and B. Siciliano. Variable Impedance Control of Redundant Manipulators for Intuitive HumanRobot Physical Interaction. *IEEE Transactions on Robotics*, Vol. 31(**4**), 850–863, 2015.

W. Khalil and E. Dombre. Modeling, Identification and Control of Robots, chapter 3 - Direct geometric model of serial robots. *Butterworth-Heinemann*, 2002.

O. Khatib. Motion/Force Redundancy of Manipulators. *In Proc. of Japan-U.S.A. Symposium on Flexible Automation*, Kyoto, Japan, 337–342, 1990.

R. Kurazume and T. Hasegawa. A new index of serial-link manipulator performance combining dynamic manipulability and manipulating force ellipsoids. *IEEE Transactions on Robotics*, Vol. 22(**5**), 1022–1028, 2006.

B-J. Lee. Geometrical derivation of differential kinematics to calibrate model parameters of flexible manipulator. *International Journal of Advenced Robotic systems*, Vol. 10, 2013.

H. Moradi and S. Lee. Joint limit analysis and elbow movement minimization for redundant manipulators using closed form method *In Proc. of Int. Conf. on Intelligent Computing*, 423–432, 2005.

M. Shimizu, H. Kakuya, W-K. Yoon and K. Kitagaki. Analytical inverse kinematic computation for 7-dof redundant manipulators with joint limits and its application to redundancy resolution. *IEEE Transactions on Robotics*, Vol. 24(**5**), 1131–1142, 2008.

D. Tolani, A. Goswami and N.I. Badler. Inverse Kinematics Techniques for Anthropomorphic Limbs. *Graphical Models*, Vol. 62(**5**), 353–388, 2000.

Y. Wang and P. Artemiadis. Closed-form inverse kinematic solution for anthropomorphic motion in redundant robot arms. *Advances in Robotics Automation*, 2014.

Y. Wu, A. Klimchik, A. Pashkevich, S. Caro and B. Furet. Optimality criteria for measurement poses selection in calibration of robot stiffness. parameters. *In Proc. of the ASME 11th Biennial Conference on Engineering Systems Design and Analysis*, Nantes, France, 1–10, 2012.

T. Yoshikawa. Manipulability of Robotic Mechanisms. *International journal of robotics research*, Vol. 4(**2**), 1985.

D. Zhou, L. Ji, Q. Zhang and X. Wei. Practical analytical inverse kinematic approach for 7-dof space manipulators with joint and attitude limits *Intelligent Service Robotics*, Vol. 8(**4**), 215–224, 2015.